Supplement of Atmos. Chem. Phys., 25, 11407–11422, 2025
https://doi.org/10.5194/acp-25-11407-2025-supplement

Atmospheric Chemistry and Physics
Open Access
EGU

Supplement of

Isotopic signatures of methane emission from oil and natural gas plants in southwestern China

Dingxi Chen et al.

Correspondence to: Longfei Yu (longfei.yu@sz.tsinghua.edu.cn)

Contents

S1 Source partitioning with end-member mixing method

In this study, we used CH_4 isotopes and mixing ratios as tracers. The contribution of atmospheric background, open surface area, and facility area to the CH_4 content of the air was calculated using the following formula:

$$\delta^{13}C_m=a\cdot\delta^{13}C_1+b\cdot\delta^{13}C_2+c\cdot\delta^{13}C_3 \quad (S1)$$

$$C_m=a\cdot C_1+ b\cdot C_2+ c\cdot C_3 \quad (S2)$$

$$1=a + b + c \quad (S3)$$

Where $\delta^{13}C_m$, $\delta^{13}C_1$, $\delta^{13}C_2$, $\delta^{13}C_3$ represent CH_4 isotopes in the air, the atmospheric background, the surface open area and the facility area, respectively; and a, b, c represent the contributions of the atmospheric background, the surface open area and the facility area, respectively; C_m, C_1, C_2, C_3 represent CH_4 mixing ratios in the air, the atmospheric background, the surface open area, and the facility area, respectively (results were shown in SI, Table S4). The values of a, b, and c can be obtained by combining equations S1, S2 and S3.

S2 Sensitivity analysis with the updated source isotope signatures of CH_4 from the Chinese ONG industry

As the isotopic signatures of major anthropogenic CH_4 sources may act as important benchmarks for estimating global emission budgets(Schwietzke et al., 2016), we applied a back-of-the-envelope calculation based on the revised isotope signatures for the Chinese ONG industry from our study. The computation processes are indicated as below:

$$Q_T = Q_{FF} + Q_{mic} + Q_{BB} \quad (S4)$$

Where Q_T, Q_{FF}, Q_{mic}, and Q_{BB} represent the total CH_4 emission of global, fossil fuel, microbial, and biomass burning sources, respectively.

$$Q_T \cdot \delta^{13}C_Q = Q_{FF} \cdot \delta^{13}C_{FF} + Q_{mic} \cdot \delta^{13}C_{mic} + Q_{BB} \cdot \delta^{13}C_{BB} \quad (S5)$$

Where $\delta^{13}C_Q$ is the combined signal of $\delta^{13}C$ emitted to the atmosphere. $\delta^{13}C_{FF}$, $\delta^{13}C_{mic}$, and $\delta^{13}C_{BB}$ represent the $\delta^{13}C$ of global fossil fuel, microbial, and biomass burning sources, respectively.

The abundance of CH_4 isotopes ($\delta^{13}C$) in the atmosphere is determined by the global sources of CH_4 and their contribution ratios, including fossil fuels (oil and natural gas, coal), biomass burning and microbial sources (wetland, ruminant, termites, rice and landfill/waste, etc.). Each source has different isotope signal values ($\delta^{13}C$); details are show in SI, Table S5, and these data were obtained from the global CH_4 isotope database(Schwietzke et al., 2016). The global ground-based CH_4 and $\delta^{13}C$ data (monthly average data) are available from the NOAA server (https://gml.noaa.gov/dv/data/). At the same time, global CH_4 emissions data are available from Saunois, M. et al.(Saunois et al., 2024).

In order to calculate the effect of this study's results on the global flux of fossil fuel, and microbial sources, we based on the following assumptions: (1) since CH_4 emissions from biomass sources are relatively small (less than 10%), the contribution ratio is constant; (2) $\delta^{13}C_{mic}$ and $\delta^{13}C_{BB}$ are also constant which from recent research; (3) the results of this study represent the $\delta^{13}C$-CH_4 (-25.66 ‰, mean values of the 11 stations) signature of the region from ONG, and we modified $\delta^{13}C_{FF}$ based on our results and weighted (Eq. (6)). Because of the timeliness of the data, we calculated the Q_{FF} and Qmic for the 2010-2019 decades with equation (4) and (5):

$$\delta^{13}C_{FF} = f_1 \cdot \delta^{13}C_1 + f_2 \cdot \delta^{13}C_{FFG} \quad \text{(S6)}$$

Where f_1 represents the ratio of CH_4 emissions from China's ONG sector to global CH_4 emissions from fossil fuel, and f_2=1-f_1. $\delta^{13}C_{FFG}$ (-44 ‰) represents the average $\delta^{13}C$ of global fossil fuel, and $\delta^{13}C_1$ -25.66 ‰) represents the average $\delta^{13}C$ of Chinese ONG sector based on this study.

The detailed calculations are shown below:

The global CH_4 emissions data from Saunois, M. et al.(Saunois et al., 2024), for 2010-2019 decades, the total emission (excluding other natural sources) was 571 Tg CH_4 yr^{-1}, the fossil fuel sources ,the biomass and burning sources and the microbial sources emission was 117.5 Tg CH_4 yr^{-1}, 27.5 Tg CH_4 yr^{-1}, and 426 Tg CH_4 yr^{-1}, respectively. So, the global contribution of fossil fuel sources, biomass and burning sources and microbial sources was 20.58%, 4.81% and 74.61%, respectively. In addition, CH_4 emissions from China's ONG industry account for approximately 2.5% of global CH_4 emissions from fossil sources(Iea, 2024). The $\delta^{13}C$ signatures of each CH_4 source from SI, Table S5.

According equation (5), (6) and relevant data above:

$\delta^{13}C_Q$= 20.58 % × (-44 ‰) + 4.81% × (-22.2 ‰) + 74.61 % × (-62.2 ‰) = -56.53 ‰; and $\delta^{13}C_{FF}$= 2.5 % × (-25.66 ‰) + 97.5 % × (-44 ‰) = -43.54 ‰;

Then, based on the relevant assumptions and equation (4) and (5), where $\delta^{13}C_Q$ = -56.53 ‰, $\delta^{13}C_{FF}$=-43.40 ‰.

Then, according equation (4), (5) and relevant data above:

$f_{FF} + f_{mic}$=95.19%; f_{FF}×(-43.54‰) + f_{mic}×(-62.2‰) + 4.81%×(-22.2‰)= -56.53‰;

Where f_{FF}, f_{mic} represent the proportions of global methane emissions from fossil fuel sources and microbial sources, respectively. From the calculations, we found that f_{FF}=20.08 %, indicated that the CH_4 emissions from fossil fuel sources was overestimated by 0.5%, this corresponds to an overestimation of emissions by 2.86 Tg CH_4 yr^{-1}. Microbial sources were underestimated to the same extent.

Table S1 The information of samples from oil and natural gas production sites

Site	Site No.	Sampling location	Date	No.	Average $\delta^{13}C$ (‰)	Average CH_4 (ppm)
MX	S1	Pipeline area	4.13	MX-01	-46.97	2.03
		H: 100 m	4.13	MX-02	-47.63	1.99
		H: 50 m	4.13	MX-03	-47.30	1.97
		H: 100 m	4.13	MX-04	-46.62	1.99
		H: 50 m	4.13	MX-05	-46.59	1.98
		Production area	4.13	MX-06	-46.08	2.01
		Ground	4.13	MX-07	-42.17	2.40
		Production area	4.13	MX-08	-46.18	2.05
SN	S2	H: 200 m	4.14	SN-01	-46.24	1.98
		H: 300 m	4.14	SN-02	-46.87	1.88
		H: 100 m	4.14	SN-03	-47.99	1.97
		Production area	4.14	SN-04	-30.41	3.49
		Production area	4.14	SN-05	-44.73	2.07
		H: 50 m	4.14	SN-06	-45.44	2.02
		H: 200 m	4.14	SN-08	-45.47	2.00
		Ground	4.14	SN-09	-45.36	2.05
		H: 50 m	4.14	SN-11	-46.71	1.97
		Pipeline area	4.14	SN-12	-31.24	3.66
		Pipeline area	4.14	SN-13	-44.31	2.22
XBQ	S3	Ground	4.15	HJB-01	-45.29	2.17
		Pipeline area	4.15	HJB-02	-47.69	2.01
		H: 300 m	4.15	HJB-03	-46.75	1.97
		H: 200 m	4.15	HJB-04	-45.56	2.06
		H: 100 m	4.15	HJB-05	-46.36	1.91
		H: 50 m	4.15	HJB-06	-47.09	1.99
XQ	S4	Ground	4.15	SZG-01	-44.90	2.15
		Pipeline area	4.15	SZG-02	-38.80	2.61
		Well	4.15	SZG-03	-45.54	2.14
		H: 300 m	4.15	SZG-04	-47.00	1.96
		H: 200 m	4.15	SZG-05	-45.75	1.88
		H: 100 m	4.15	SZG-06	-45.57	2.03
		H: 50 m	4.15	SZG-07	-45.47	1.91
DQ	S5	Ground	4.16	NMG-01	-46.71	2.00
		Pipeline area	4.16	NMG-02	-44.40	1.99
		H: 300 m	4.16	NMG-03	-46.77	1.98
		H: 200 m	4.16	NMG-04	-46.50	1.98
		H: 100 m	4.16	NMG-05	-47.04	1.98
		H: 50 m	4.16	NMG-06	-46.23	1.95
XM	S6	Ground	4.16	XM-01	-46.19	1.98

Table S1 continued

		Pipeline area	4.16	XM-02	-46.88	1.99
		H: 300 m	4.16	XM-03	-45.50	2.14
		H: 200 m	4.16	XM-04	-45.64	2.14
		H: 100 m	4.16	XM-05	-48.14	1.98
		H: 50 m	4.16	XM-06	-45.42	2.01
QTCSN	S7	Ground	4.17	QTC-01	-44.02	2.24
		Pipeline area	4.17	QTC-02	-36.98	2.95
		H: 300 m	4.17	QTC-03	-45.16	2.05
		H: 200 m	4.17	QTC-04	-46.96	2.00
		H: 100 m	4.17	QTC-05	-45.63	2.15
		H: 50 m	4.17	QTC-06	-47.32	2.00
QTCSZ	S8	Ground	4.17	QTCSZ-01	-45.69	2.15
		Pipeline area	4.17	QTCSZ-02	-39.79	2.45
		H: 300 m	4.17	QTCSZ-03	-44.93	2.05
		H: 200 m	4.17	QTCSZ-04	-45.95	2.14
		H: 100 m	4.17	QTCSZ-05	-45.24	2.14
		H: 50 m	4.17	QTCSZ-06	-44.37	2.09
LHZ	S9	Ground	4.18	LHZ-01	-44.89	2.17
		Pipeline area	4.18	LHZ-02	-45.22	2.17
		H: 300 m	4.18	LHZ-03	-46.89	1.98
		H: 200 m	4.18	LHZ-04	-44.11	2.13
		H: 100 m	4.18	LHZ-05	-45.67	2.02
		H: 50 m	4.18	LHZ-06	-47.60	1.99
L1	S10	Ground	4.18	L1-01	-43.38	2.06
		Pipeline area	4.18	L1-02	-44.86	2.19
		H: 300 m	4.18	L1-03	-44.57	2.15
		H: 200 m	4.18	L1-04	-44.30	2.04
		H: 100 m	4.18	L1-05	-46.02	2.13
		H: 50 m	4.18	L1-06	-44.86	2.02
ZYZ	S11	Ground	4.19	ZHZ-01	-47.34	1.98
		Pipeline area	4.19	ZHZ-02	-44.75	2.10
		H: 300 m	4.19	ZHZ-03	-45.15	2.00
		H: 200 m	4.19	ZHZ-04	-45.50	2.04
		H: 100 m	4.19	ZHZ-05	-46.33	1.99
		H: 50 m	4.19	ZHZ-06	-44.39	2.13
Well		Leak	4.11	YJ-01	-16.19	118.98
		Leak	4.11	YJ-02	-24.52	47.00
		Ground	4.11	YJ-03	-40.26	2.79
Urban		Park	4.12	GY-01	-45.47	2.15
		Park	4.12	GY-02	-46.25	2.03
		Riverside	4.12	GY-03	-46.31	1.99
		Riverside	4.12	GY-04	-46.79	1.99

Table S2 $\delta^{13}C$ in major ONG basins of China

Basin	Area	Production layer	$\delta^{13}C_{CH4}$ (‰)	Reference
Tarim Basin	Platform area of Tarim Basin	O	-42.6~ -32	(Liu et al., 2019)
Sichuan Basin	Sichuan Basin	C, P, T	-37~ -27	
Ordos Basin	Lower Paleozoic of Ordos Basin	O	-40.3~ -31	
Liaohe Basin	Western part of Liaohe Depression	E	-54.8~ -31	(Huang et al., 2017)
Huanghua Depression	Huanghua Depression	E	-47.3~ -36.8	(Wang et al., 2015)
Tarim Basin	Platform area of Tarim Basin	∈, O	-45.4~ -32.0	
Sichuan Basin	Northeastern Sichuan Basin	S	-32.5~ -27.0	
Songliao Basin	Songliao	J-K	-32.7~ -17.4	(Yang et al., 2008)
Sichuan Basin	Wolonghe Field	T, P, C	-34.5~ -31.69	(Cai et al., 2013)
Sichuan Basin	Weiyuan Field	Z	-32.38~ -32.37	
Sichuan Basin	East Sichuan Basin	P, T	-34.5~ -28.9	
Sichuan Basin	East Sichuan Basin	T	-32.35~ -29.52	(Cai et al., 2004)
Sichuan Basin	Northeastern Sichuan Basin	P, T	-37.44~ -29.4	(Hao et al., 2008)
Zhujiangkou	Panyu30-1	N	-33.89	(Zhu et al., 2014)
Tarim Basin	Tazhong Uplift	O	-54.9~ -35.7	(Wang et al., 2018)
Sichuan Basin	Sichuan Basin	Z, ∈, C, P, T	-37.9~ -28.5	(Zhang et al., 2018)

Table S3 The results of HYSPLIT model and meteorological station at sites

sites	Ground		H: 50 m		H: 100 m		H: 200 m		H: 300 m	
	Wind speed (m/s)	Wind direction	Wind speed (m/s)	Wind direction	Wind speed (m/s)	Wind direction	Wind speed (m/s)	Wind direction	Wind speed (m/s)	Wind direction
S1	2.85/1.4	33.5°/155°	4.11	32°	3.54	32.9°	4.28	32.9°	4.00	38.2°
S2	1.69/1.63	265.7°/169°	1.75	265.2°	1.82	265.0°	1.88	264.6°	1.34	263.3°
S3	2.21/0.95	70.4°/180°	2.39	71.9°	2.60	74.8°	2.83	76.9°	3.08	86.0°
S4	2.67/1.36	164.9°/183°	3.28	165.8°	2.76	167.5°	3.65	168.5°	2.86	170.8°
S5	2.21/0.89	70.4°/157°	2.39	71.9°	2.60	74.8°	2.83	76.9°	3.08	86.0°
S6	2.67/1.38	113.1°/160°	2.73	113.9°	2.76	115.8°	2.89	116.5°	2.86	117.5°
S7	0.89/0.73	73.8°/118°	1.06	75°	1.18	94.5°	1.58	100.5°	1.93	125.2°
S8	1.98/0.96	67°/207°	1.97	68˚	2.03	67.6˚	2.12	67˚	1.93	70.4˚
S9	1.69/1	265.7°/213°	1.75	265.2˚	1.82	265.0˚	1.88	264.6˚	1.34	263.3˚
S10	1.33/1.1	259.2°/194°	1.46	261.3˚	1.50	264.0˚	1.74	267.5˚	1.68	270.9˚
S11	1.81/0.71	145.0°/228°	1.91	144.1˚	2.05	143.2˚	2.29	144.4˚	2.39	142.2˚

The table above shows data from the HYSPLIT model and meteorological stations. There were models and measurements data on the ground and only simulations at high altitudes. “XX/XX” stands for “output of HYSPLIT model/measured of metrological station” values on the ground. The measured values are expressed as mean values; both the modeled and measured results were compared, showing general correlation, although the surface meteorological conditions are complex and changeable. This means that HYSPLIT's simulation results are reliable.

Table S4 The results of source partitioning at sites

Site	Heights	Atmospheric background (%)	Ground (%)	Facility area (%)
S1	50 m	44	0	56
	100 m	/	/	/
S2	50 m	94	0	6
	100 m	/	/	/
	200 m	40	60	0
	300 m	100	0	0
S3	50 m	39	14	47
	100 m	/	/	/
	200 m	0	55	45
	300 m	66	20	14
S4	50 m	93	0	7
	100 m	75	10	15
	200 m	96	0	4
	300 m	83	17	0
S5	50 m	47	26	27
	100 m	30	70	0
	200 m	19	70	11
	300 m	12	88	0
S6	50 m	/	/	/
	100 m	/	/	/
	200 m	/	/	/
	300 m	/	/	/
S7	50 m	/	/	/
	100 m	80	0	20
	200 m	94	0	6
	300 m	85	0	15
S8	50 m	72	0	28
	100 m	18	70	12
	200 m	70	0	30
	300 m	80	0	20
S9	50 m	/	/	/
	100 m	51	49	0
	200 m	/	/	/
	300 m	76	0	24
S10	50 m	36	51	13
	100 m	27	0	73
	200 m	/	/	/
	300 m	22	59	19
S11	50 m	/	/	/

Table S4 continued

100 m	38	28	4
200 m	26	6	68
300 m	40	0	60

"/" represents the $\delta^{13}C$ of target value (air) which is higher or lower than the source value (atmospheric background, open surface area and facility area), and it cannot be calculated, only qualitative analysis can be performed.

Table S5 $\delta^{13}C$ signatures of each CH_4 source(Schwietzke et al., 2016)

sources	Mean of $\delta^{13}C$ (‰)
Fossil fuel	-44
Microbial	-62.2
Biomass burning	-22.2

S3 Instrument calibration

The CRDS system from Picarro used in our research has been widely applied for measuring CH_4 isotopic signatures from various sources (Menoud et al., 2022; Ars et al., 2024; Al-Shalan et al., 2022; Geum et al., 2024; Rella et al., 2015; Lu et al., 2021). Actually, we should note that, we have used two international primary standards (based on VPDB; Std1 and Std2, -68.6‰ and -40.0‰) and one secondary standards (House-standards, Hstd, -46.89‰) which had been cross-calibrated. Along each measurement sequence (see more details as demonstrated in the figure S1), we measure all three standards together with the standards (5 samples for each sequence), during which Std 1 is used for calibration and correction for sequence-drift, Std 2 used for quality control and Hstd used for constraining long-term drift. As for our case, the measurements were finished within less than a week, so we didn't correct for long-term drift. For simplicity consideration, we only adopted Std 1 for calibration (both delta calibration and short-term drift correction). Of course, the short-term drift was minor compared with delta calibration.

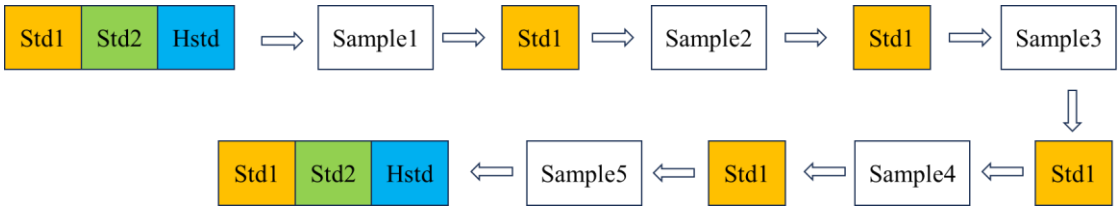

Fig. S1 Methane Isotopic Analysis Procedure for Gas Samples

In addition, the measurement results of the Std1 standard gas were recorded over a period of more than one year to evaluate the long-term stability and reliability of the instrument (From January 18, 2023, to May 23, 2024) (Figure S2).

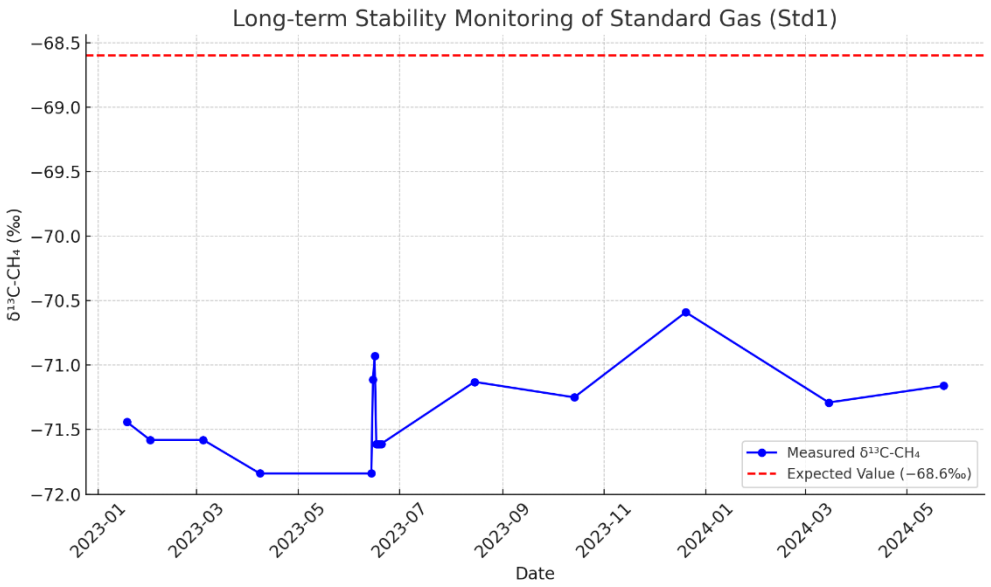

Fig. S2 This figure presents the variation in measured δ^{13}C-CH_4 values of the standard gas (Std1) from January 18, 2023, to May 23, 2024. The red dashed line indicates the theoretical value of the standard gas (−68.6‰), while the blue line represents the actual measurements obtained from the instrument. The absence of a significant drift trend suggests that the instrument exhibited good long-term stability over the monitoring period.

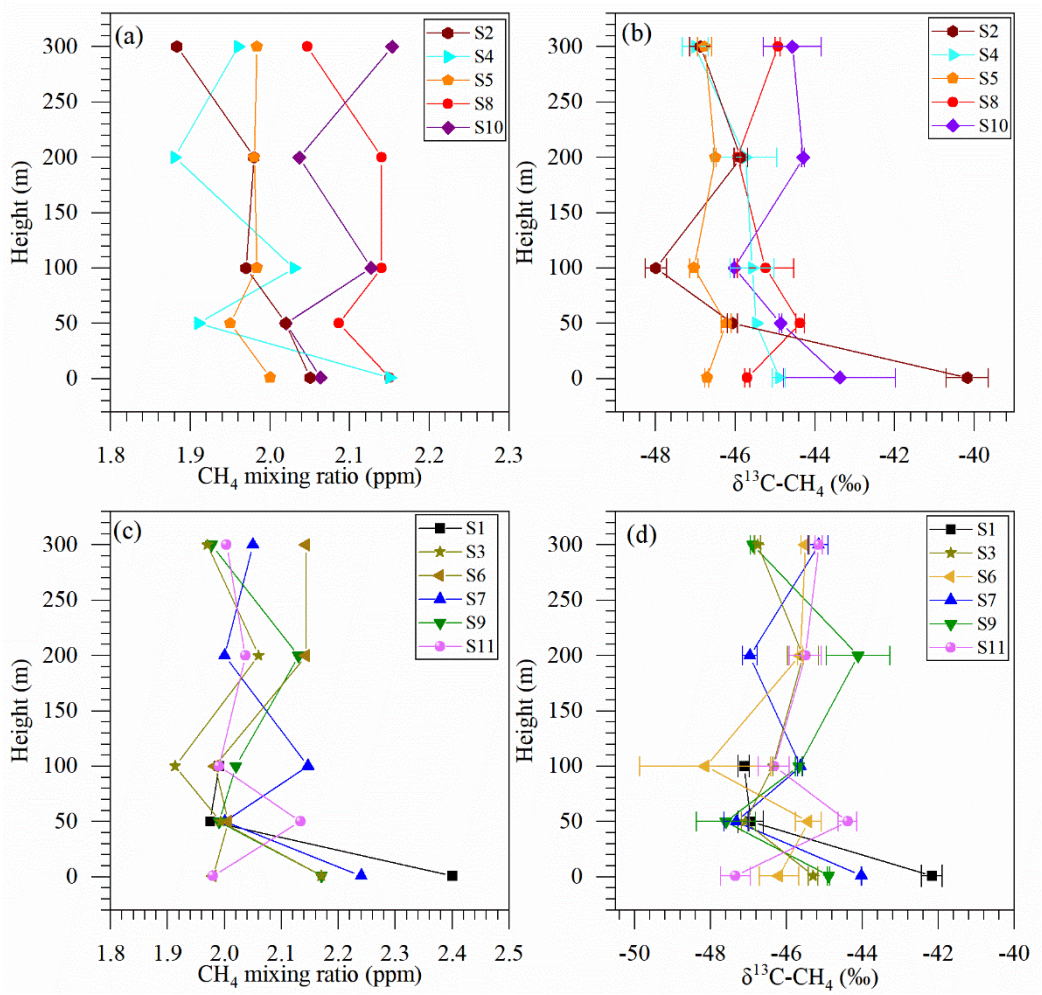

Fig. S3 Vertical variation characteristics of CH_4 mixing ratios (a, c) and isotopes (b, d) at different field stations; because of the sampling accident, only 50 m and 100 m altitude data are obtained from S1 field station, and the other stations obtained full altitude data. The variation trend of CH_4 mixing ratio and isotope vertical profile of S1, S3, S6, S7, S9, S11 and S2, S4, S5, S8, S10 sites were shown in the picture (c, d) and (a, b), respectively.

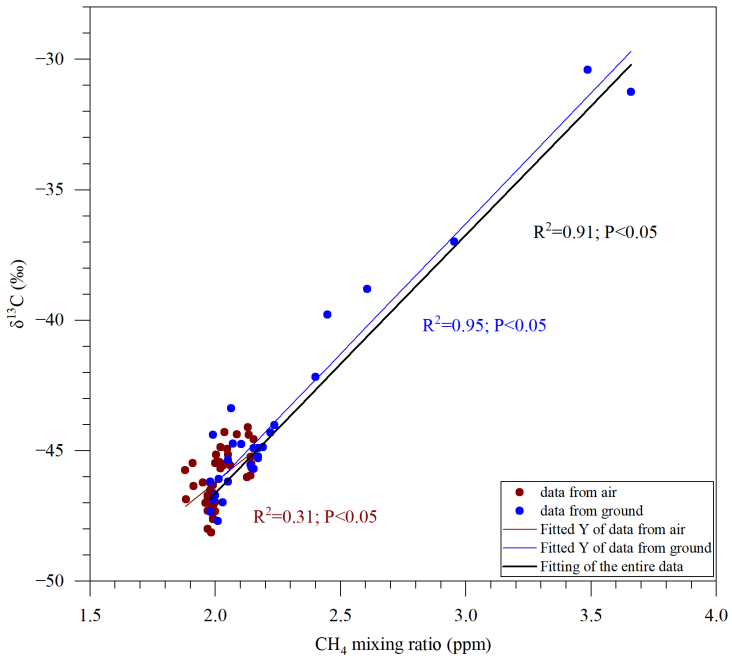

Fig. S4 Linear fit of CH_4 mixing ratios to isotopes, data from 11 sites CH_4 samples. Green and red points represent air data and ground data, respectively; black, green and red lines represent integral fitting line, fitting line of ground and air, respectively; R^2 values are 0.91 (a), 0.95 (b), and 0.31 (c), $P<0.05$, respectively. The slopes of the black and green line are very close, almost coinciding.

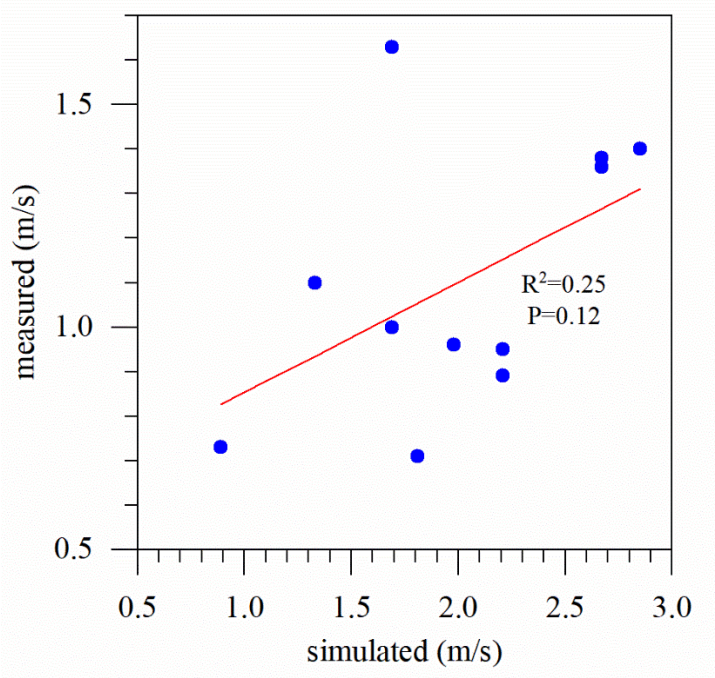

Fig. S5 The fitting analysis of the wind speed based on the HYSPLIT model and meteorological station.

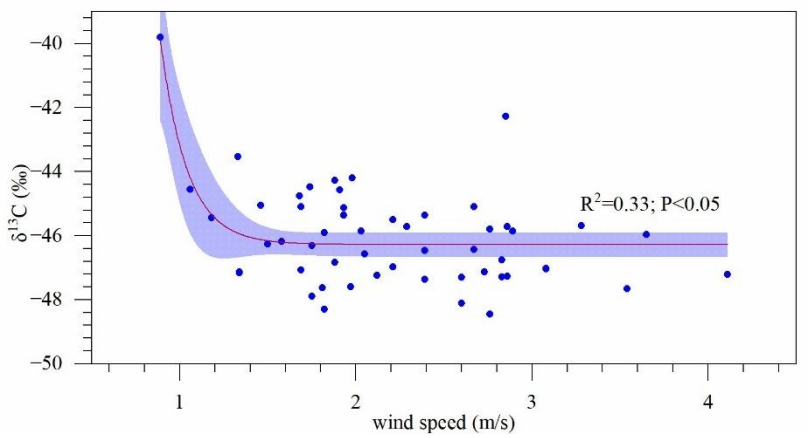

Fig. S6 Exponential correlation between wind speed and isotopes of site, wind speed and isotope data at different altitudes are included, and R^2 is 0.33, P<0.05. The blue area represents the 95% confidence interval and red lines represent fitting line.

Meteorological conditions, particularly wind direction, exert a significant influence on the distribution of CH_4 at the stations. The application of the HYSPLIT model is essential for understanding this phenomenon. The following example illustrates the impact of wind direction on CH_4 distribution at S7 station. During the investigation, a leak source was identified in the northeast direction of the facility area (CH_4 mixing ratios from 2.3 ppm to 13 ppm during the monitoring period). Given that the wind direction in the area where the S7 station is located was northeast, a significant increase in CH_4 mixing ratio was observed in the southwest direction of the facility area.

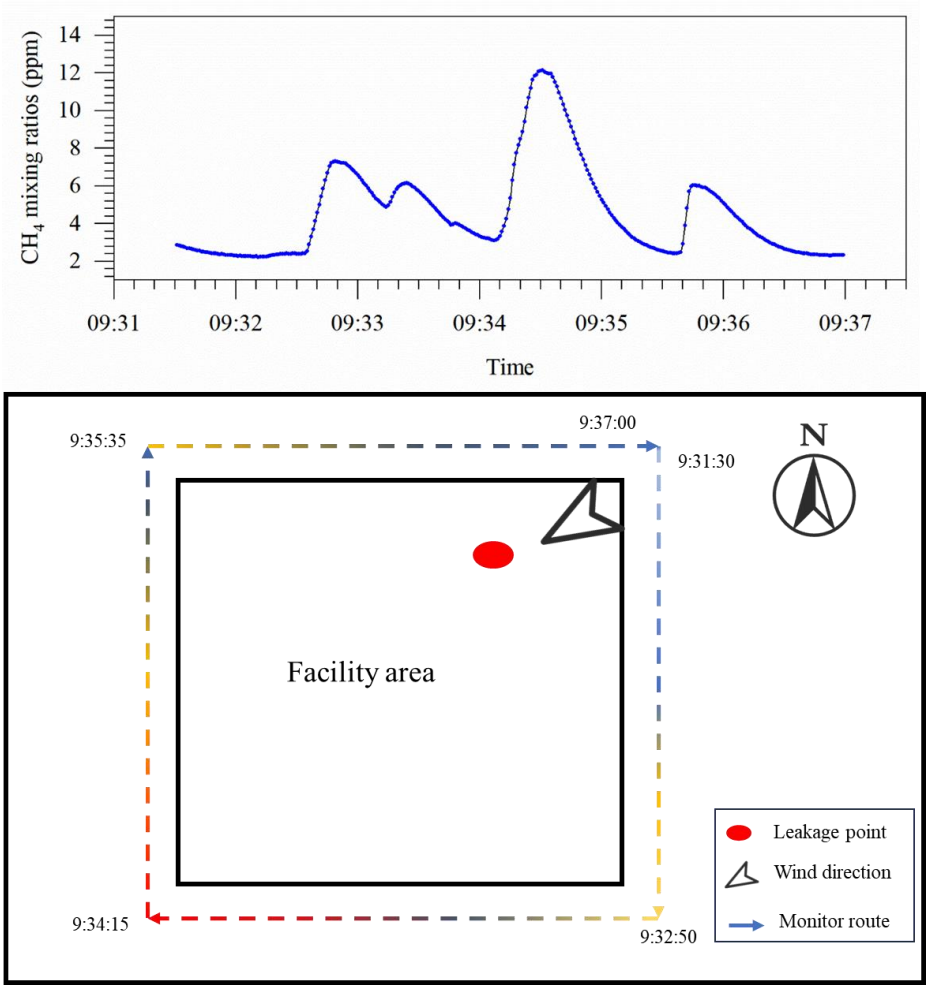

Fig. S7 Impact of meteorological conditions on the distribution of CH_4 at station S7. The upper figure shows a time-mixing ratios relationship for monitoring, while the lower figure illustrates a schematic of site monitor (schematic provided for confidentiality reasons). The dashed line indicates the monitor route, with colors representing CH_4 mixing ratios: blue for low (2~3 ppm), orange for medium (3~7 ppm), and red for high (7~12 ppm).

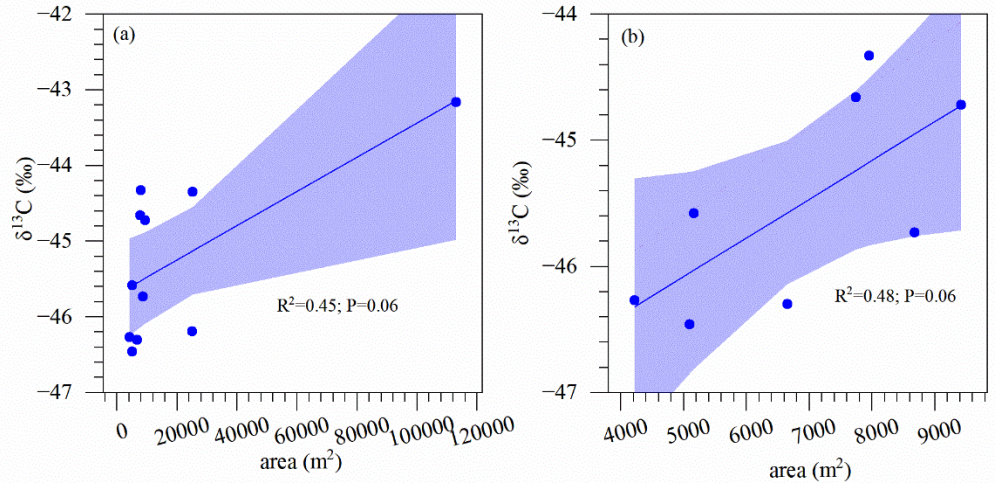

Fig. S8 Correlation between size and isotopes of the site. The fitting relation of all field stations (a), and part of sites which area are less than 10000 m^2; R^2 and P values

are 0.45 and 0.06 (a), 0.48 and 0.06 (b), respectively. The blue area represents the 95% confidence interval and red lines represent fitting line.

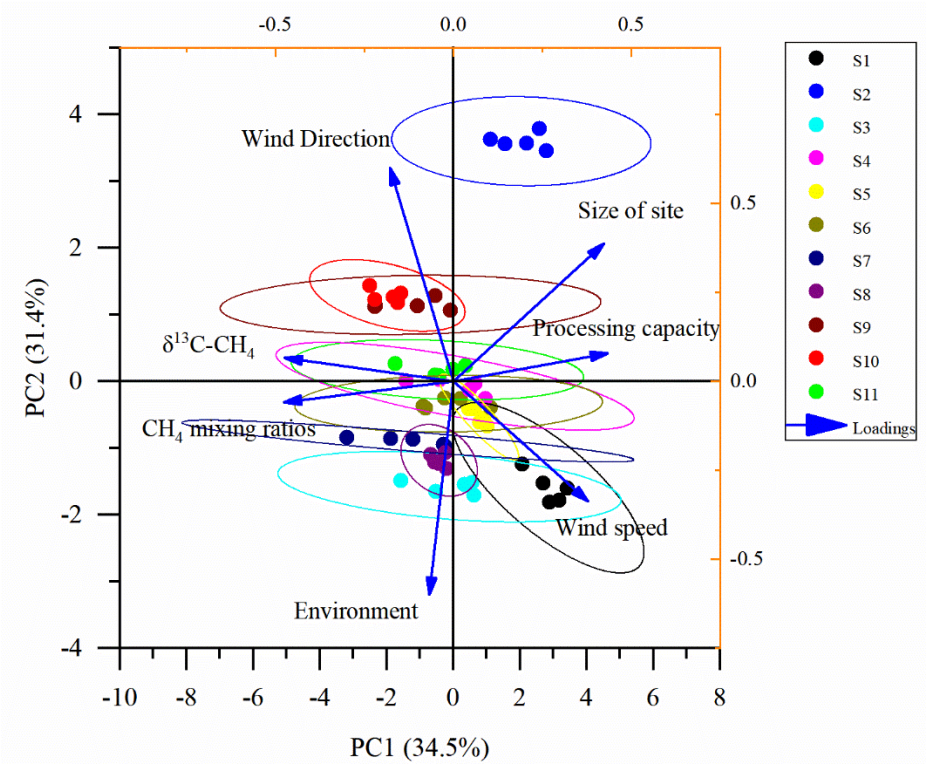

Fig. S9 Principal Component Analysis (PCA) of influencing factors of CH_4 isotope ($\delta^{13}C$) and mixing ratio in the field station. Including wind speed and direction, surrounding environment, size of the site and processing capacity.

References

Al-Shalan, A., Lowry, D., Fisher, R. E., Nisbet, E. G., Zazzeri, G., Al-Sarawi, M., and France, J. L.: Methane emissions in Kuwait: Plume identification, isotopic characterisation and inventory verification, Atmospheric Environment, 268, 118763, https://doi.org/10.1016/j.atmosenv.2021.118763, 2022.

Ars, S., Arismendi, G. G., Muehlenbachs, K., Worthy, D. E. J., and Vogel, F.: Using in situ measurements of δ13C in methane to investigate methane emissions from the western Canada sedimentary basin, Atmospheric Environment: X, 23, 100286, https://doi.org/10.1016/j.aeaoa.2024.100286, 2024.

Cai, C., Zhang, C., He, H., and Tang, Y.: Carbon isotope fractionation during methane-dominated TSR in East Sichuan Basin gasfields, China: A review, Marine and Petroleum Geology, 48, 100-110, 2013.

Cai, C., Xie, Z., Worden, R. H., Hu, G., Wang, L., and He, H.: Methane-dominated thermochemical sulphate reduction in the Triassic Feixianguan Formation East Sichuan Basin, China: towards prediction of fatal H2S concentrations, Marine and Petroleum Geology, 21, 1265-1279, 2004.

Geum, S., Park, H., Choi, H., Kim, Y., Lee, H., Joo, S., Oh, Y.-S., Michel, S. E., and Park, S.: Identifying emission sources of CH4 in East Asia based on in-situ observations of atmospheric δ 13C-CH4 and C2H6, Science of The Total Environment, 908, 168433, https://doi.org/10.1016/j.scitotenv.2023.168433, 2024.

Hao, F., Guo, T., Zhu, Y., Cai, X., Zou, H., and Li, P.: Evidence for multiple stages of oil cracking and thermochemical sulfate reduction in the Puguang gas field, Sichuan Basin, China, AAPG bulletin, 92, 611-637, 2008.

Huang, S., Feng, Z., Gu, T., Gong, D., Peng, W., and Yuan, M.: Multiple origins of the Paleogene natural gases and effects of secondary alteration in Liaohe Basin, northeast China: Insights from the molecular and stable isotopic compositions, International Journal of Coal Geology, 172, 134-148, 2017.

Global Methane Tracker 2025: https://www.iea.org/reports/global-methane-tracker-2024, last

Liu, Q., Wu, X., Wang, X., Jin, Z., Zhu, D., Meng, Q., Huang, S., Liu, J., and Fu, Q.: Carbon and hydrogen isotopes of methane, ethane, and propane: A review of genetic identification of natural gas, Earth-Science Reviews, 190, 247-272, 2019.

Lu, X., Harris, S. J., Fisher, R. E., France, J. L., Nisbet, E. G., Lowry, D., Röckmann, T., van der Veen, C., Menoud, M., Schwietzke, S., and Kelly, B. F. J.: Isotopic signatures of major methane sources in the coal seam gas fields and adjacent agricultural districts, Queensland, Australia, Atmos. Chem. Phys., 21, 10527-10555, 2021.

Menoud, M., van der Veen, C., Maazallahi, H., Hensen, A., Velzeboer, I., van den Bulk, P., Delre, A., Korben, P., Schwietzke, S., Ardelean, M., Calcan, A., Etiope, G., Baciu, C., Scheutz, C., Schmidt, M., and Röckmann, T.: CH4 isotopic signatures of emissions from oil and gas extraction sites in Romania, Elementa: Science of the Anthropocene, 10, 2022.

Rella, C. W., Hoffnagle, J., He, Y., and Tajima, S.: Local- and regional-scale measurements of CH₄, δ¹³CH₄, and C₂H₆ in the Uintah Basin using a mobile stable isotope analyzer, Atmos. Meas. Tech., 8, 4539-4559, 10.5194/amt-8-4539-2015, 2015.

Saunois, M., Martinez, A., Poulter, B., Zhang, Z., Raymond, P., Regnier, P., Canadell, J. G., Jackson,

R. B., Patra, P. K., Bousquet, P., Ciais, P., Dlugokencky, E. J., Lan, X., Allen, G. H., Bastviken, D., Beerling, D. J., Belikov, D. A., Blake, D. R., Castaldi, S., Crippa, M., Deemer, B. R., Dennison, F., Etiope, G., Gedney, N., Höglund-Isaksson, L., Holgerson, M. A., Hopcroft, P. O., Hugelius, G., Ito, A., Jain, A. K., Janardanan, R., Johnson, M. S., Kleinen, T., Krummel, P., Lauerwald, R., Li, T., Liu, X., McDonald, K. C., Melton, J. R., Mühle, J., Müller, J., Murguia-Flores, F., Niwa, Y., Noce, S., Pan, S., Parker, R. J., Peng, C., Ramonet, M., Riley, W. J., Rocher-Ros, G., Rosentreter, J. A., Sasakawa, M., Segers, A., Smith, S. J., Stanley, E. H., Thanwerdas, J., Tian, H., Tsuruta, A., Tubiello, F. N., Weber, T. S., van der Werf, G., Worthy, D. E., Xi, Y., Yoshida, Y., Zhang, W., Zheng, B., Zhu, Q., Zhu, Q., and Zhuang, Q.: Global Methane Budget 2000-2020, Earth Syst. Sci. Data Discuss., 2024, 1-147, 10.5194/essd-2024-115, 2024.

Schwietzke, S., Sherwood, O. A., Bruhwiler, L. M. P., Miller, J. B., Etiope, G., Dlugokencky, E. J., Michel, S. E., Arling, V. A., Vaughn, B. H., White, J. W. C., and Tans, P. P.: Upward revision of global fossil fuel methane emissions based on isotope database, Nature, 538, 88-91, 2016.

Wang, X., Liu, W., Shi, B., Zhang, Z., Xu, Y., and Zheng, J.: Hydrogen isotope characteristics of thermogenic methane in Chinese sedimentary basins, Organic Geochemistry, 83-84, 178-189, 2015.

Wang, Y., Chen, J., Pang, X., Zhang, B., Chen, Z., Zhang, G., Luo, G., and He, L.: Origin of deep sour natural gas in the Ordovician carbonate reservoir of the Tazhong Uplift, Tarim Basin, northwest China: Insights from gas geochemistry and formation water, Marine and Petroleum Geology, 91, 532-549, 2018.

Yang, C., Luo, X., Li, J., Li, Z., Liu, Q., and Wang, Y.: Geochemical characteristics of pyrolysis gas from epimetamorphic rocks in the northern basement of Songliao Basin, Northeast China, Science in China Series D: Earth Sciences, 51, 140-147, 2008.

Zhang, S., He, K., Hu, G., Mi, J., Ma, Q., Liu, K., and Tang, Y.: Unique chemical and isotopic characteristics and origins of natural gases in the Paleozoic marine formations in the Sichuan Basin, SW China: Isotope fractionation of deep and high mature carbonate reservoir gases, Marine and Petroleum Geology, 89, 68-82, 2018.

Zhu, G., Wang, Z., Dai, J., and Su, J.: Natural gas constituent and carbon isotopic composition in petroliferous basins, China, Journal of Asian Earth Sciences, 80, 1-17, 2014.